Optical and Quantum Electronics (2021) 53:222
https://doi.org/10.1007/s11082-021-02896-x

Synthesis and characterization of tin (IV) oxide thin films

M. Rahayi[1] · M. H. Ehsani[1] · Agnes C. Nkele[2] · M. M. Shahidi[1] · Fabian I. Ezema[2,3,4]

Received: 2 December 2020 / Accepted: 12 April 2021 / Published online: 21 April 2021

Abstract

Tin (IV) oxide, SnO_2 films have been successfully synthesized in argon gas using a magnetron sputtering device. The morphology, structure, optical, photoluminescence, and photoresponse features of the samples have been analyzed via field electron scanning electron microscope, X-ray diffractograms, UV–Vis spectrometer, and spectro fluorophotometer. Compact nano grained morphologies with tetragonal structure and high absorbance were obtained. Increasing the annealing temperature led to a slight rise in the bandgap energies of the deposited samples. SnO_2 films exhibited good photoluminescence features with increasing photoresponse with time as the annealing temperature reduced. The films can be potentially applied to optical and solar cell devices.

Graphic abstract

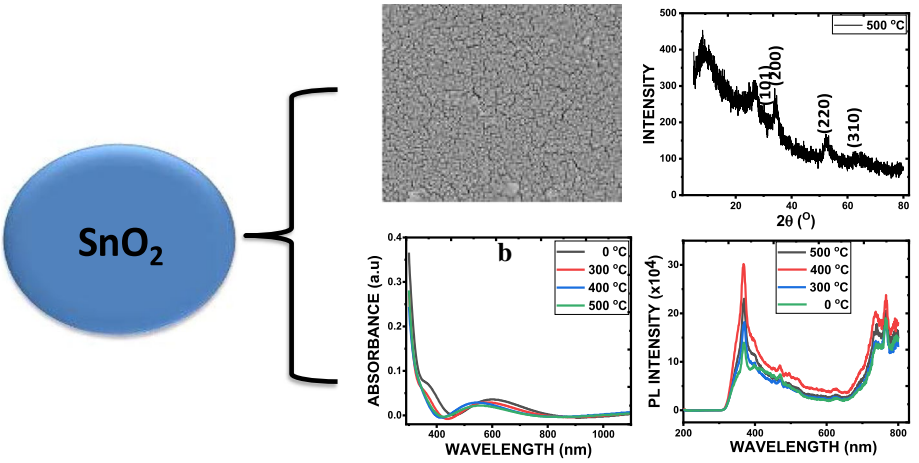

✉ M. H. Ehsani
ehsani@semnan.ac.ir

1 Faculty of Physics, Semnan University, 35195-363 Semnan, Iran

2 Department of Physics and Astronomy, University of Nigeria, Nsukka, Enugu, Nigeria

3 Nanosciences African Network (NANOAFNET), iThemba LABS-National Research Foundation, 1 Old Faure road, P.O. Box 722, Somerset West 7129, Western Cape, South Africa

4 UNESCO-UNISA Africa Chair in Nanosciences/Nanotechnology, College of Graduate Studies, University of South Africa (UNISA), Muckleneuk ridge, P.O. Box 392, Pretoria, South Africa

Keywords Tin (IV) oxide · Sputtering · Tetragonal · Annealing · Solar cells

1 Introduction

Transparent conducting oxides (TCOs) have been researched because they exhibit combined optical and electrical features that grant them useful access in batteries, sensing devices, optoelectronics, solar cells, and photocatalyst devices (Batzill and Diebold 2005). Tin (IV) oxide is an important TCO that undergoes phase transition during the synthesis process, has a transparent conducting surface, great sensitivity, and a useful catalyst during oxidation processes (Batzill and Diebold 2005). The different forms of fabricating SnO_2 sensors could be as whiskers, pallets, thick or thin films (Mitra and Mondal 2008). Tin (IV) oxide is an n-type semiconducting material with good stability, oxidation state of + 4, has a wide and direct bandgap (Eifert et al. 2017), high conductivity (Kılıç and Zunger 2002), great optical features (Kang 2010), and can exist in the tetragonal or orthorhombic phase. It finds useful application in optical devices, solar cells, gas sensors, perovskite cells, and dye-sensitized solar cells (Kumara et al. 2001).

Several methods of synthesizing tin (IV) oxide films include chemical bath deposition (Amma et al. 2005), spray deposition (Baranauskas et al. 2005; Kasar et al. 2008; Chacko 2006; Thangaraju 2002), successive ionic layer adsorption and reaction (Mitra and Mondal 2008; Deshpande et al. 2008; Pusawale et al. 2011), evaporation technique (Geurts et al. 1984; Jaiswal et al. 2013), sequential infiltration synthesis (Barick et al. 2019), ion beam irradiation (Kang 2010), chemical vapor deposition (Nagirnyak et al. 2016; Naeem et al. 2015), magnetron sputtering (Adamchuk et al. 2019; Chub et al. 2020), atomic layer deposition (Mai 2019; Maximov 2017). The diverse synthesis methods influence the quality and properties exhibited by the films. Sputter deposition allows film materials to be ejected from a target to a substrate with minimal heating effects. Sputtered films adhere more on substrate surfaces, sputter materials of high melting point, and produce films with similar compositions as the source material. Annealing films improve the crystal structure, enhances surface features, reduces strain, and improves optical features (Nkele 2019). Tin (IV) oxide films are usefully applied in optoelectronic, catalytic devices (Barick et al. 2019), and sensors (Chub et al. 2020).

Several works have been carried out on the synthesis of SnO_2 by the sputtering technique. Sangaletti et al. (1997) thermally treated tin films in the air via RF sputtering to obtain a mixed orthorhombic and tetragonal phase. Camacho-Lopéz (2013) characterized reactive DC-sputtered SnO_2 film and obtained tetragonal-phased and high transmittance films. The purpose of this research is to synthesize and characterize the obtained morphologies, structure, optical, and photoluminescence characteristics of the sputtered tin (IV) oxide films.

2 Experimental details

2.1 Materials and methods

The SnO_2 material was synthesized on the glass substrate via an RF magnetron sputtering device. SnO_2 ceramic target (Kurt. J. Lesker, 99.99% pure) and 2 mm diameter with 6 mm thickness was deposited by RF power supply. First, the substrates were cleaned

intensively before coating. The layering stage was performed in the argon (99.99% pure) atmosphere. The chamber was first vacuumed by a turbo molecular pump to an initial pressure of 5×10^{-5} torr while the working pressure was kept constant at 4.5×10^{-3} torr. Before starting the coating process, the chamber was flashed thrice with argon (Ar) gas to eliminate oxygen and other contaminants from the chamber. A thin film of SnO_2 with a power of 80 watts was layered to a thickness of 100 nm. After coating, the samples were heated at 300 °C (S3), 400 °C (S2) and 500 °C (S1) for 2 h in the air atmosphere. One sample (S4) was left without heating treatment.

The Au metal interdigital electrodes (IDEs) were deposited on the prepared SnO_2 samples by the sputtering technique as schematically illustrated in Fig. 1. The thickness and active area of the patterned IDEs were kept constant at 100 nm and 3.5 mm^2, respectively.

2.2 Characterizations

The synthesized tin (IV) oxide films were respectively analyzed to understand the morphology, structure, optical, photoluminescence, and photoresponse features using field electric scanning electron microscope (FESEM) (Sigma 300-HV Zeiss), X-ray diffraction (XRD) (ADVANCE-D8 Bruker) equipped with $Cu_{k\alpha}$ radiation source with $\lambda = 1.5406$ Å, UV–Vis spectrometer (1800 UV/Vis SHIMADZU), Spectro fluorophotometer (RF-6000 SHIMADZU). I–V features of the films were obtained at room temperature and atmospheric pressure. The LED was blue with 0.11 W/m^2 intensity with 2 min OFF/ON switching cycles under 5 V bias voltage.

3 Results and discussion

3.1 Morphological studies

FESEM images revealed tiny clusters of nanoparticles distributed over the substrate surface, as seen in Fig. 2. Similar tiny morphology has also been reported by Barick et al. (2019). Synthesizing the SnO_2 film produced clustered nano grains evenly distributed with surface cracks. The surface cracks are usually attributed to SnO_2 films because developing oxide films leads to stress development in the films. The cracks could also be due to

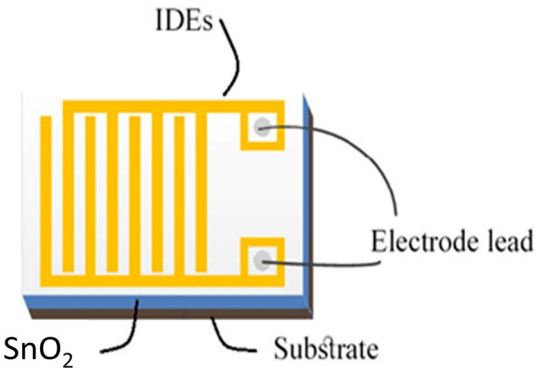

Fig. 1 Schematic of the interdigitated electrode and SnO_2 thin film device

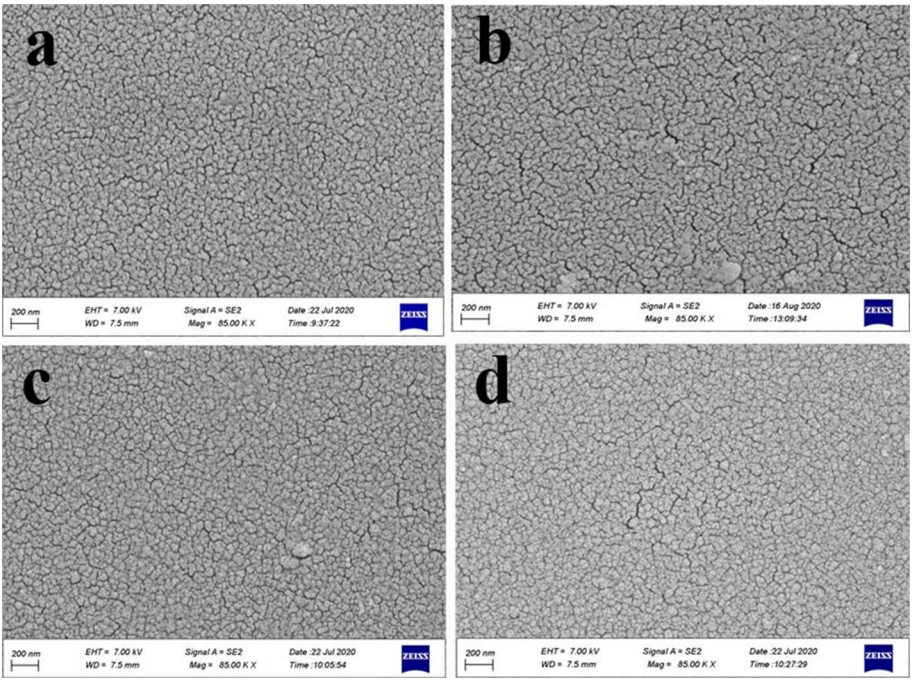

Fig. 2 FESEM images of the films synthesized at **a** 500 **b** 400 **c** 300 **d** 0 °C

deposition conditions, low surface porosity, and diffusion of oxygen into the pores of the oxide layer (Camacho-López et al. 2013).

A cross-section of the FESEM images for the synthesized films has been shown in Fig. 3a–d. Uniform film distribution can be observed throughout the substrate surface

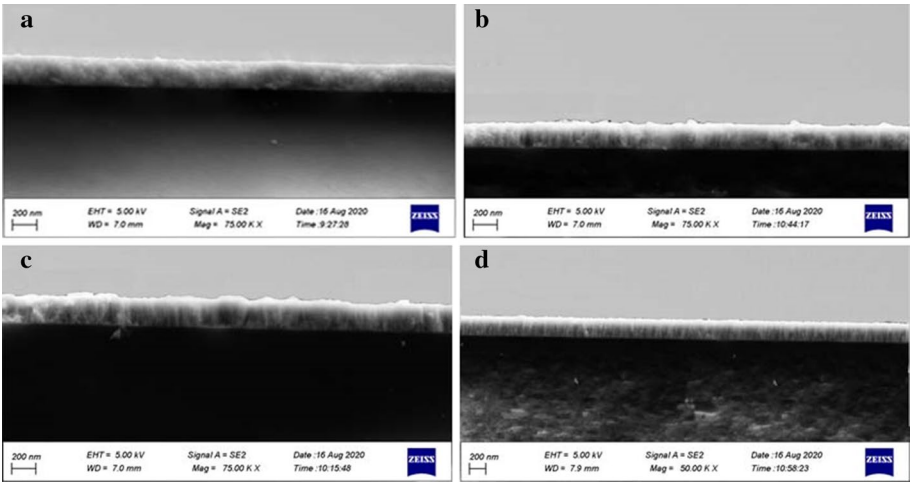

Fig. 3 Cross-sectional FESEM images of the films synthesized at **a** 500 **b** 400 **c** 300 **d** 0 °C

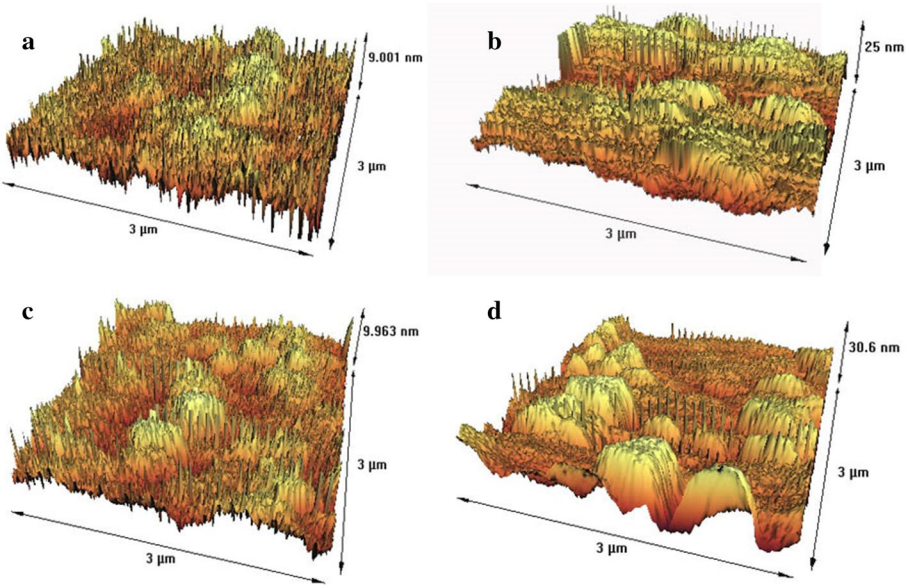

Fig. 4 AFM images of the samples synthesized at **a** 500 **b** 400 **c** 300 **d** 0 °C

Table 1 Roughness values for the deposited films

Samples (°C)	R_a (nm)	R_q (nm)
500	1.09	1.40
400	1.66	2.16
300	1.19	1.53
0	1.72	2.20

with efficient material build-up. The most annealed film recorded the highest optical transparency due to the applied post-heating effect. This property makes the films useful in optical devices and light-emitting diodes (Kang 2010).

Atomic force microscope images of the films obtained at several temperatures in tapping modes are shown in Fig. 4a–d. Round homogenous bulges were seen as agglomerations on the substrate surface. Spikes of different densities emanating from the substrate surface can be observed at varying temperatures. Varying the annealing temperature significantly affected the density of the tin (IV) oxide nanostructures. Thickness values of 240 nm, 219 nm, 210 nm, and 200 nm were obtained for the SnO_2 films annealed respectively at 0 °C, 300 °C, 400 °C, and 500 °C with the help of Digimizer software program. The film's thickness decreased with increasing annealing temperature because the thermal energy overcomes the adhesion and bonding energies of loosely bound atoms, thereby reducing the number of atoms that are adsorbed on the surface.

The roughness values for the samples were obtained using Eqs. (1) and (2) and are displayed in Table 1.

$$R_a = \frac{1}{n}\sum y_i \tag{1}$$

$$R_q = \sqrt{\frac{1}{n}\sum y_i^2} \tag{2}$$

It can be observed that the unannealed film recorded the maximum roughness value while the film annealed at 500 °C had the least roughness value. Increasing the annealing temperature led to more growth of the nanoclusters, and accounts for the thickness variations.

3.2 Structural analysis

Figure 5 displays a tetragonal crystalline structure of the SnO_2 films at 2theta degrees ranging from 10° to 80°. The lattice planes of the X-ray diffractograms and their corresponding 2theta angles are 26.57° (1 1 0), 33.86° (1 0 1), 37.94° (2 0 0), 51.76° (2 1 1), 54.74° (2 2 0), 57.81° (0 0 2), 61.86° (3 1 0), 64.72° (1 1 2), 71.26° (2 0 2), 78.68° (3 2 1). Tamilalagan et al. (2020) obtained similar lattice planes. The non-distinct peaks were indicative of sputtered tin (IV) oxide films (Popovich et al. 2016). Applying low and high temperatures to tin oxide produced poorly crystalline films (Singh 2019). Annealing the films led to a

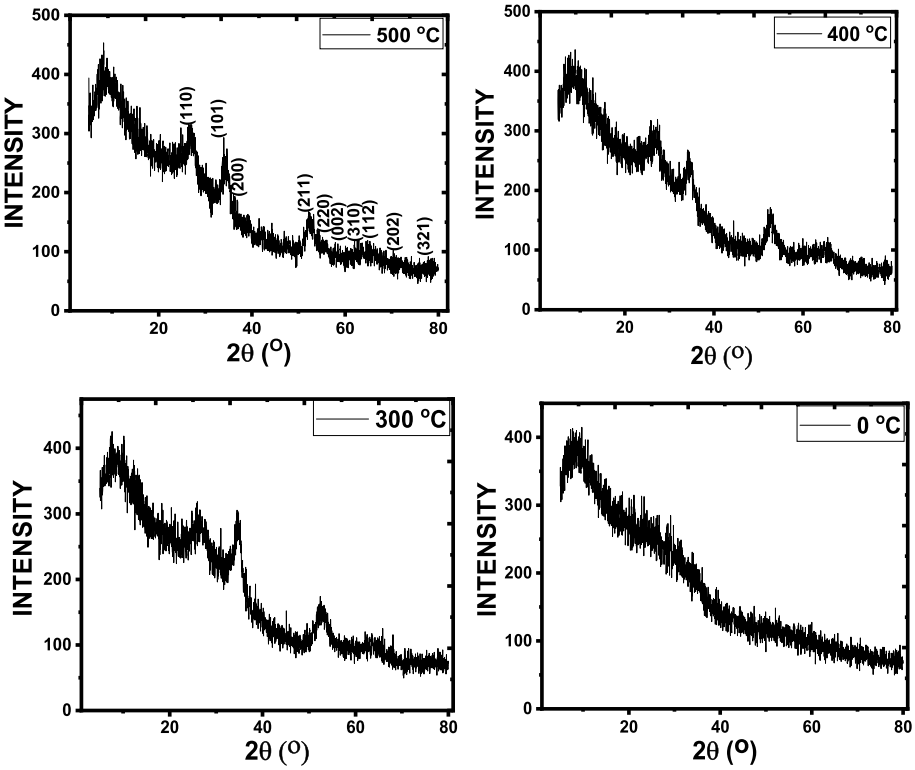

Fig. 5 Structural patterns of the SnO_2 films synthesized at varying temperatures

transformation to the polycrystalline tin (IV) oxide phase, reduction of water content, and stabilization the TiO_2 structure (Adamchuk et al. 2019). The structural parameters obtained from the most prominent peaks have been outlined in Table 2.

Table 2 showed that increasing the annealing temperature reduced the crystallite size, D and interplanar distance, d. The decreasing crystallite size could be attributed to the high density of the localized state. The lattice constants, a and c have also been outlined in Table 2, where the lattice constant a equals that of b.

3.3 Optical studies

Figure 6 gives the optical transmittance, absorbance, and reflectance plots for the deposited films. The deposited films recorded high transmittance and absorbance. The films were transparent to light in the visible electromagnetic spectrum. Reduced and fluctuating reflectance values were observed at increasing wavelength regions. Annealing the films reduced the reflectance of the films in the visible spectrum. Similar transmittance and absorbance features have been reported in the literature (Singh 2019; Ivanova 2020). These optical features make the SnO_2 films potential materials for solar cells.

The absorption coefficient versus wavelength plot of the SnO_2 films are exhibited in Fig. 7a. A similar absorption coefficient trend was obtained with the most annealed film recording the highest absorption. Figure 7b shows the bandgap energy plots of the synthesized films. Tauc plot was employed in determining the bandgap energies of the films. The bandgap energy values of the films increased from 3.18 to 3.21 eV as the annealing temperature increased, due to confinement of the electrons and holes. Subjecting the films to annealing conditions did not significantly alter the band structure of the films (Bazargan et al. 2012). Similar results have also been obtained (Sangaletti 1997; Kong et al. 2010).

3.4 Photoluminescence (PL) studies

Photoluminescence analysis is a non-destructive technique that gives information on the optical, point defects, and photochemical features of the films under study. Figure 8 provides the photoluminescence plot of the unannealed and annealed SnO_2 films measured at a PL wavelength of 200 nm. The unannealed sample exhibited higher photoluminescence quenching than the annealed samples. Maximum PL emission occurred at 369 nm within the visible emission region. Strong emission bands were obtained at 369 nm and 766 nm, while weak emission bands were visible at 470 nm, 626 nm, and 739 nm. The unannealed sample exhibited lower luminous intensity than the annealed samples; thereby making the heat-treated SnO_2 films suitable for optical materials. The role of oxygen vacancies in PL analysis is evident from the decrease in PL intensity (Nehru et al. 2012).

Table 2 Some structural parameters for the SnO_2 films

Temp. (°C)	2θ (°)	hkl	D (Å)	d (Å)	a (Å)	c (Å)
0	26.74	110				
300	34.38	011	53.00	3.33	4.65	3.15
400	52.51	121	39.00	2.61	4.65	3.16
500	63.29	211	31.00	1.74	4.69	3.17

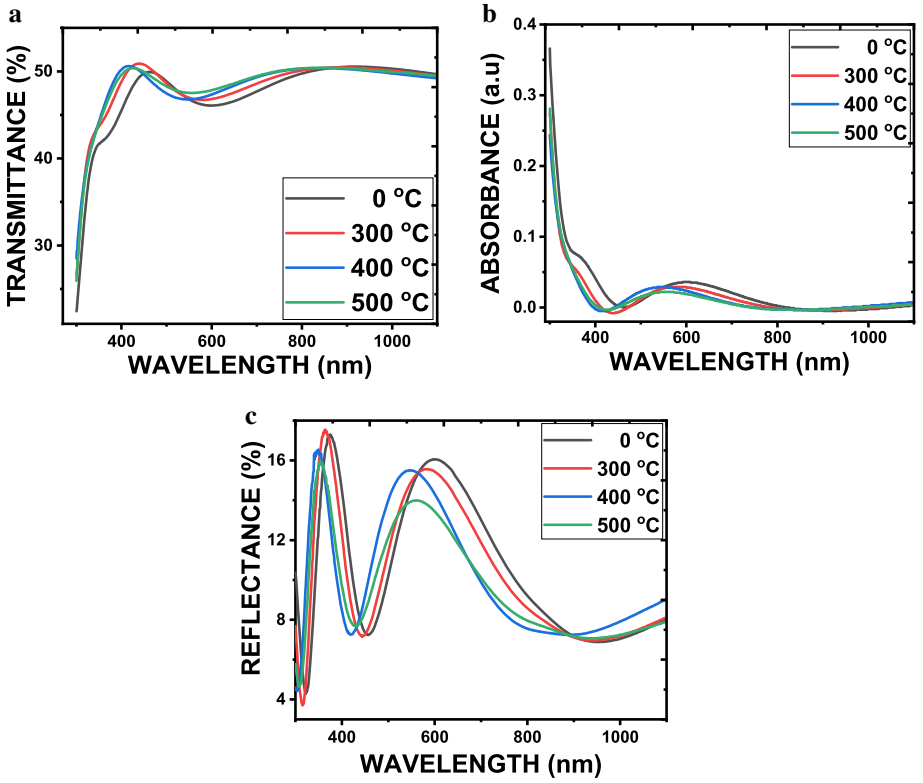

Fig. 6 Optical **a** transmittance, **b** absorbance, and **c** reflectance plots of the synthesized samples

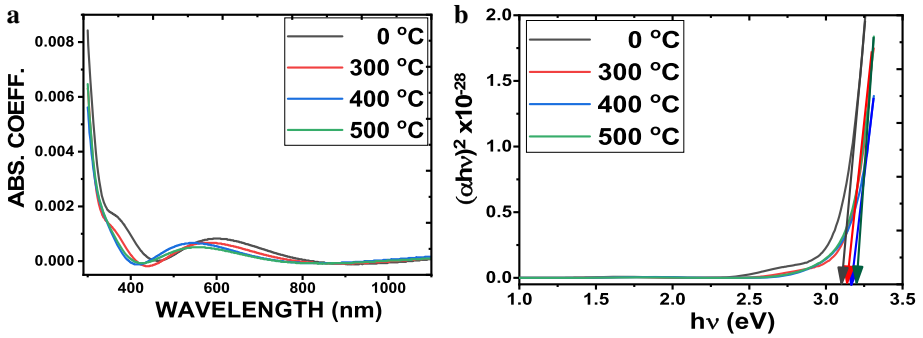

Fig. 7 Plots showing the **a** absorption coefficient and **b** bandgap energies of the samples

3.5 Photoresponse analysis

The photoresponse (current versus time) plots of the films are shown in Fig. 9. Figure 9 depicts the time-dependent photoresponse behavior when the devices are under darkness and irradiation by blue lights with 2 min OFF/ON switching cycles under 5 V bias voltage.

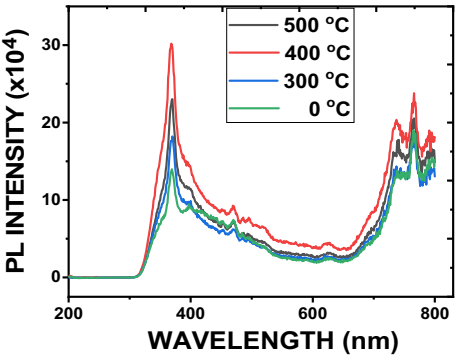

Fig. 8 Photoluminescence spectra of the deposited films

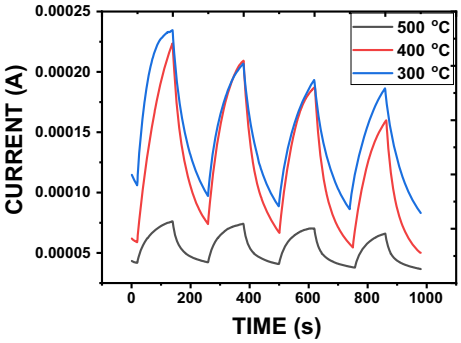

Fig. 9 Plot showing the photoresponse spectra of the annealed SnO_2 films

Table 3 Photoresponse parameters of the samples

SnO_2 (Temperature)	R (AW^{-1})$\times 10^2$	D* (jones)$\times 10^9$
300	2.7	5.6
400	2.7	7.1
500	8.4	4.6

The more the annealing temperature, the better the photoresponse of the films (Breddels and Blasse 1984). The film annealed at 500 °C recorded the best photoresponse as outlined in Table 3.

The photocurrent I_{ph} is defined in Eq. (3) (Tian and Fan 2018) as:

$$I_{ph} = I_{illuminated} - I_{dark} \tag{3}$$

Two parameters of photodetector are calculate (Zhong 2017):

$$\text{Photo responsivity (R)} = I_{ph}/PS \tag{4}$$

$$\text{Detectivity}(D*) = [(RS)^1/2]/[(2eIdark)^1/2] \tag{5}$$

where I_{ph} is the photocurrent, P is the light power intensity, and S is the effective exposure area of the photodetector, and I_{dark} is the dark current. The results obtained are displayed in Table 1.

Table 3 shows increased photoresponse of the tin (IV) oxide films at the higher annealing temperatures. The sample annealed at 400 °C recorded the highest photodetection ability because more photogenerated carriers were created at that temperature. This increased sensitivity makes SnO_2 films useful as sensors (Bazargan et al. 2012; Savaniu 1999).

4 Conclusion

This work successfully synthesized SnO_2 films unannealed and annealed at 300 °C, 400 °C, and 500 °C via the RF magnetron sputtering technique. The films were characterized for their morphological, structural, optical, photoluminescence, and photoresponse features. The unannealed film had compact nanog rained morphology with surface cracks, while AFM images showed spikes emanating from the substrate surface. The films exhibited a tetragonal crystal structure with the high absorbance feature. The bandgap energy value of the SnO_2 films increased with annealing temperature. The highest photoluminescence intensity was recorded at 369 nm within the visible electromagnetic region. The films also recorded good photoresponse to current. The synthesized SnO_2 films could be potentially applied in optical and solar cell devices.

References

Adamchuk, D.V., Ksenevich, V.K., Poklonski, N.A., Navickas, M., Banys, J.: Nonstoichiometric tin oxide films: study by X-ray diffraction, Raman scattering and electron paramagnetic resonance. Lith. J. Phys. (2019). https://doi.org/10.3952/physics.v59i4.4138

Amma, D.S.D., Vaidyan, V.K., Manoj, P.K.: Structural, electrical and optical studies on chemically deposited tin oxide films from inorganic precursors. Mater. Chem. Phys. **93**(1), 194–201 (2005). https://doi.org/10.1016/j.matchemphys.2005.03.045

Baranauskas, V., Fontana, M., Guo, Z.J., Ceragioli, H.J., Peterlevitz, A.C.: Field-emission properties of nanocrystalline tin oxide films. Sens. Actuators B Chem. **107**(1), 474–478 (2005). https://doi.org/10.1016/j.snb.2004.11.004

Barick, B.K., Simon, A., Weisbord, I., Shomrat, N., Segal-Peretz, T.: Tin oxide nanostructure fabrication via sequential infiltration synthesis in block copolymer thin films. J. Colloid Interface Sci. **557**, 537–545 (2019). https://doi.org/10.1016/j.jcis.2019.09.044

Batzill, M., Diebold, U.: The surface and materials science of tin oxide. Prog. Surf. Sci. **79**(2–4), 47–154 (2005)

Bazargan, S., Heinig, N.F., Rios, J.F., Leung, K.T.: Electronic transport in tin(IV) oxide nanocrystalline films: two-medium transport with three-dimensional variable-range hopping mechanism for the ultrasmall nanocrystallite size regime. J. Phys. Chem. C **116**(8), 4979–4985 (2012). https://doi.org/10.1021/jp209864e

Breddels, P.A., Blasse, G.: Photoelectrochemical studies of thin films of several tetraphenylporphyrins deposited on tin(IV) oxide electrodes. J. Chem. Soc. Faraday Trans. **80**(9), 1055–1065 (1984). https://doi.org/10.1039/F29848001055

Camacho-López, M.A., Galeana-Camacho, J.R., Esparza-García, A., Sánchez-Pérez, C., Julien, C.M.: Characterization of nanostructured SnO2 films deposited by reactive DC-magnetron sputtering. Superficies y vacío **26**(3), 95–99 (2013)

Chacko, S., Bushiri, M.J., Vaidyan, V.K.: Photoluminescence studies of spray pyrolytically grown nanostructured tin oxide semiconductor thin films on glass substrates. J. Phys. D Appl. Phys. **39**(21), 4540–4543 (2006). https://doi.org/10.1088/0022-3727/39/21/004

Chub, I., Pirogov, O., Mirgorod, O., Rudakov, S.: Investigation of the gas sensitive properties of tin dioxide films obtained by magnetron sputtering. Mater. Sci. Forum **1006**, 239–244 (2020)

Deshpande, N.G., Vyas, J.C., Sharma, R.: Preparation and characterization of nanocrystalline tin oxide thin films deposited at room temperature. Thin Solid Films **516**(23), 8587–8593 (2008). https://doi.org/10.1016/j.tsf.2008.06.016

Eifert, B., et al.: Raman studies of the intermediate tin-oxide phase. Phys. Rev. Mater. (2017). https://doi.org/10.1103/PhysRevMaterials.1.014602

Geurts, J., Rau, S., Richter, W., Schmitte, F.J.: SnO films and their oxidation to SnO_2: Raman scattering, IR reflectivity and X-ray diffraction studies. Thin Solid Films **121**(3), 217–225 (1984). https://doi.org/10.1016/0040-6090(84)90303-1

Ivanova, A., et al.: Cellulose nanocrystal-templated tin dioxide thin films for gas sensing. ACS Appl. Mater. Interfaces **12**(11), 12639–12647 (2020). https://doi.org/10.1021/acsami.9b11891

Jaiswal, M.K., Kanjilal, D., Kumar, R.: Structural and optical studies of 100MeV Au irradiated thin films of tin oxide. Nucl. Instrum. Methods Phys. Res. Sect. B **314**, 170–175 (2013). https://doi.org/10.1016/j.nimb.2013.05.053

Kang, Y.-G., et al.: Superior optical properties of homogeneous liquid crystal alignment on a tin (IV) oxide surface sequentially modulated via ion beam irradiation. Opt. Exp. OE **18**(21), 21594–21602 (2010). https://doi.org/10.1364/OE.18.021594

Kasar, R.R., Deshpande, N.G., Gudage, Y.G., Vyas, J.C., Sharma, R.: Studies and correlation among the structural, optical and electrical parameters of spray-deposited tin oxide (SnO_2) thin films with different substrate temperatures. Phys. B **403**(19), 3724–3729 (2008). https://doi.org/10.1016/j.physb.2008.06.023

Kılıç, Ç., Zunger, A.: Origins of coexistence of conductivity and transparency in SnO_2. Phys. Rev. Lett. **88**(9), 095501 (2002)

Kong, L., Ma, J., Zhu, Z., Luan, C., Yu, X., Yu, Q.: Synthesis of orthorhombic structure epitaxial tin oxide film. Mater. Lett. **64**(12), 1350–1353 (2010)

Kumara, G.R.R.A., Tennakone, K., Perera, V.P.S., Konno, A., Kaneko, S., Okuya, M.: Suppression of recombinations in a dye-sensitized photoelectrochemical cell made from a film of tin IV oxide crystallites coated with a thin layer of aluminium oxide. J. Phys. D Appl. Phys. **34**(6), 868–873 (2001). https://doi.org/10.1088/0022-3727/34/6/306

Mai, L., et al.: Low-temperature plasma-enhanced atomic layer deposition of tin(IV) oxide from a functionalized alkyl precursor: fabrication and evaluation of SnO_2-based thin-film transistor devices. ACS Appl. Mater. Interfaces **11**(3), 3169–3180 (2019). https://doi.org/10.1021/acsami.8b16443

Maximov, MYu., et al.: Characterization and electrochemical performance at high discharge rates of tin dioxide thin films synthesized by atomic layer deposition. J. Electron. Mater. **46**(11), 6571–6577 (2017). https://doi.org/10.1007/s11664-017-5701-8

Mitra, P., Mondal, S.: Hydrogen and LPG sensing properties of SnO2 films obtained by direct oxidation of SILAR deposited SnS. Bull. Polish Acad. Sci. Tech. Sci. **56**, 295–300 (2008)

Naeem, R., et al.: Electric-field aerosol-assisted CVD: synthesis, characterization, and properties of tin oxide microballs prepared from a single source precursor. Chem. Vapor Depos. **21**(10-11–12), 360–368 (2015). https://doi.org/10.1002/cvde.201507178

Nagirnyak, S.V., Lutz, V.A., Dontsova, T.A., Astrelin, I.M.: Synthesis and characterization of Tin(IV) oxide obtained by chemical vapor deposition method. Nanoscale Res. Lett. **11**(1), 343 (2016). https://doi.org/10.1186/s11671-016-1547-x

Nehru, L.C., Swaminathan, V., Sanjeeviraja, C.: Photoluminescence studies on nanocrystalline tin oxide powder for optoelectronic devices. Am. J. Mater. Sci. **2**(2), 6–10 (2012)

Nkele, A.C., et al.: Structural, optical and electrochemical properties of SILAR-deposited zirconium-doped cadmium oxide thin films. Mater. Res. Exp. (2019). https://doi.org/10.1088/2053-1591/ab31f5

Popovich, A.A., Maximov, MYu., Nazarov, D.V., Novikov, P.A., Silin, A.O., Shamshurin, A.I.: Low-temperature deposition of tin(IV) oxide films for thin-film power sources. Russ. J. Appl. Chem. **89**(5), 805–808 (2016). https://doi.org/10.1134/S1070427216050190

Pusawale, S.N., Deshmukh, P.R., Lokhande, C.D.: Chemical synthesis and characterization of hydrous tin oxide (SnO_2:H_2O) thin films. Bull. Mater. Sci. **34**(6), 1179–1183 (2011). https://doi.org/10.1007/s12034-011-0168-3

Sangaletti, L., et al.: Microstructure and morphology of tin dioxide multilayer thin film gas sensors. Sens. Actuators B Chem. **44**(1–3), 268–274 (1997)

Savaniu, C., et al.: Tin dioxide sol-gel derived films doped with platinum and antimony deposited on porous silicon. Thin Solid Films **349**(1), 29–35 (1999). https://doi.org/10.1016/S0040-6090(99)00141-8

Singh, M., et al.: Facile synthesis of composite tin oxide nanostructures for high-performance planar perovskite solar cells. Nano Energy **60**, 275–284 (2019). https://doi.org/10.1016/j.nanoen.2019.03.044

Tamilalagan, E., et al.: A sonochemical assisted synthesis of hollow sphere structured tin (IV) oxide on graphene oxide sheets for the low-level detection of environmental pollutant mercury in biological samples and foodstuffs. Ultrason. Sonochem. **67**, 105164 (2020). https://doi.org/10.1016/j.ultsonch.2020.105164

Thangaraju, B.: Structural and electrical studies on highly conducting spray deposited fluorine and antimony doped SnO_2 thin films from $SnCl_2$ precursor. Thin Solid Films **402**(1), 71–78 (2002). https://doi.org/10.1016/S0040-6090(01)01667-4

Tian, H., Fan, C.: Hydrothermal synthesis and fast photoresponsive characterization of SnS_2 hexagonal nanoflakes. J. Mater. Sci. (2018). https://doi.org/10.1007/s10853-018-2959-z

Zhong, M., et al.: High-performance photodetectors based on Sb_2S_3 nanowires: wavelength dependence and wide temperature range utilization. Nanoscale **9**(34), 12364–12371 (2017)